Highly Crystallized Tungsten Trioxide Loaded Titania Composites prepared by Using Ionic Liquids and their Photocatalytic Behaviors

Ezaki, Masato
Department of Nanoscience, Sojo University

Kusakabe, Katsuki
Department of Nanoscience, Sojo University

https://doi.org/10.5109/1495159

出版情報：Evergreen. 1 (2), pp.18-24, 2014-09. 九州大学グリーンアジア国際リーダー教育センター
バージョン：

Highly Crystallized Tungsten Trioxide Loaded Titania Composites prepared by Using Ionic Liquids and their Photocatalytic Behaviors

Masato Ezaki, Katsuki Kusakabe*

Department of Nanoscience, Sojo University, 4-22-1 Ikeda, Nishi-ku, Kumamoto 860-0082, Japan

*Author to whom correspondence should be addressed,
E-mail: kusakabe@nano.sojo-u.ac.jp

(Received June 30, 2014; accepted August 6, 2014)

TiO_2/WO_3 (Ti-W) photocatalysts were prepared by a simple one-step sol-gel method with 1-butyl-3-methylimidazolium ionic liquids ([Bmim][PF_6] and [Bmim][BF_4]). The mixed sol of WO_3 derived from peroxotungstic acid and TiO_2 containing ionic liquid was dried and followed by calcination at 800°C. The resulting Ti-W composite indicated high crystallinity of WO_3 and no crystalline transformation of TiO_2 from anatase to rutile. WO_3 nanoparticles on Ti-W composites (Ti-W[PF_6]) prepared by using water immiscible [Bmim][PF_6] were highly dispersed due to an emulsification effect. Ti-W[PF_6] indicated the highest reactivity in the photodegradation of methylene blue (MB) under visible light irradiation and the photooxidation of As(III) under UV irradiation.

Keywords : Photooxidation, Ionic liquid, Tungsten trioxide, Arsenic, Sol-gel, Titania

1. Introduction

Titanium dioxide is well known to indicate an excellent photocatalytic activity under UV irradiation. When TiO_2 is utilized in the residential environment such as under daylight and room light conditions, the photocatalytic activity is reduced owing to little absorption in the visible light region. In addition when the level of pollutants is very low, the reaction is controlled by the molecular diffusion of the pollutants toward the photocatalyst and the electron-hole pair created on the TiO_2 surface can combine easily, leading to the reduction of photocatalytic activity. Modification of TiO_2 photocatalyst is necessary to solve the above disadvantages[1,2].

Anatase TiO_2 has a band gap of around 3.2 eV and therefore absorbs only 3-4 % of sunlight below 387 nm[3]. Many research works have been done in preparation of visible light active photocatalysts by doping of nitrogen, carbon or sulfur to TiO_2[4-6] and by coupling of TiO_2 with active semiconductors to the visible light[7]. Semiconductor photocatalyst WO_3 with a band gap of 2.8 eV, corresponding to absorption to approximately 500 nm, has attracted much interest[8,9]. TiO_2/WO_3 composite is a suitable photocatalyst with visible light absorption due to the stability of these oxides and the absolution positions of their band gap[10-12].

Performance of TiO_2/WO_3 photocatalyst is considered to be highly dependent on its crystalline structure and the dispersibility of WO_3 on TiO_2. These properties are strongly affected by calcination temperature. Generation and growth of WO_3 crystal are promoted by high calcination temperature. Meanwhile, the crystal transformation of TiO_2 from anatase to rutile is also induced at the high temperature. Therefore rutile TiO_2 with low catalytic activity as well as crystalline WO_3 was formed through high temperature calcination of TiO_2/WO_3 precursors. Anatase is more advantageous for photocatalytic reaction because of having highly band gap derived from the unstable crystal structure.

On the other hand, anatase TiO_2 as well as amorphous WO_3 with low visible light absorption efficiency was formed through low temperature calcination. Accordingly, the preparation of anatase TiO_2 and crystalline WO_3 composite is desirable for the visible-light sensitive photocatalyst. In the previous paper[13], crystalline WO_3 nanoparticles were synthesized by acid precipitation and the subsequent calcination at 800°C and then added into titania sol. Thus crystalline TiO_2/WO_3 composite was obtained from the calcination of the mixed suspension at 400°C.

Ionic liquid (IL) has attracted much attention for the application in the field of electrochemistry due to their high ionic conductivity and their wide electrochemical potential window[14]. It has exclusively many attractive properties, including their negligible vapor pressure, chemical stability and non-flammability. Recently, ionic liquids capable of dissolving both organic and inorganic

species have been widely used as media for organic synthesis, catalytic reaction and sol-gel process[15]. Ionic liquids in sol-gel process are known to act as drying control chemical additives, catalysts, structure directing agents and solvent[16-19]. Nanostructured TiO_2 particles were synthesized via sol-gel method by using 1-butyl-3-methylimidazolium ionic liquid[20]. The obtained TiO_2 particles were thermally stable and thus resistant to the anatase-rutile phase transformation at high calcination temperature. The anatase crystal structure was maintained up to the calcination temperature of 800°C.

In the present study, a simple one-step sol-gel method with an ionic liquid template was used to prepare a WO_3 -loaded titania (Ti-W) photocatalyst. Tungsten was introduced into TiO_2 photocatalyst by adding poly tungstic acid precursor solution to a titania sol. The reactivity of Ti-W photocatalysts in liquid phase was investigated on the degradation of methylene blue (MB) and the photooxidation of trivalent arsenic compound both under UV and visible light irradiation[21-22].

2. Experimental

2.1 Chemicals and Materials

Methylene blue (Merck), $NaAsO_2$ (As(III), Wako) and $Na_2HAsO_4{\cdot}7H_2O$ (As(V), Wako) were chosen as the model pollutant compound. Titanium tetraisopropoxide (TTIP, Ti-$(OCH(CH_3)_2)_4$, Tokyo Chemical Industry) and tungstic acid (H_2WO_4, Sigma-Aldrich) were used as a TiO_2 and WO_3 sources, respectively. Two types of imidazolium-based ionic liquids, (1-butyl-3-methylimidazolium hexafluorophosphate [Bmim][PF_6], and 1-butyl-3-methylimidazolium tetrafluoroborate [Bmim][BF_4], Sigma-Aldrich,), were used for the inhibition of the anatase-rutile phase transformation during calcination. All chemicals were used with no further purification.

Titania sol containing IL was prepared by a sol-gel method based closely on that of Choi et al.[20]. Titanium tetraisopropoxide was added into ethanol at an EtOH/TTIP molar ratio of 30. IL was then added into the mixture at an IL/TTIP molar ratio of 3 and the mixed solution was vigorously stirred for 10 min. It was observed that the solution became emulsion when water immiscible [Bmim][PF_6] was added. TiO_2 powder was obtained from the hydrolysis of TTIP. The resulting sol was also ready for the preparation of Ti-W composite sol.

5.0 g of H_2WO_4 was dissolved into 30 mL of aqueous H_2O_2 solution (30 wt%) and the obtained solution was completely dried at 50°C to obtain peroxotungstic acid powder. The peroxotungstic acid powder was re-dissolved into 5.3 mL of aqueous EtOH solution (33.3 vol%). The resulting poly tungstic acid precursor solution and the titania sol containing IL were mixed under stirring for 1 h. Water was slowly added into the mixture, stirred vigorously for 30 min. The yellow precipitate recovered by filtration was washed thoroughly with water and dried at 100°C for 2 h. The residual IL and organic compounds were removed from the dried powder by extraction with acetonitrile for 6 h. Then, the powder was recovered again by filtration and washed with acetonitrile and water several times. The resulting Ti-W composite was dried at room temperature for 18 h. The Ti-W composites synthesized by using [Bmim][PF_6] and [Bmim][BF_4] were hereafter abbreviated as Ti-W[PF_6] and Ti-W[BF_4], respectively.

2.2 Characterization

Surface morphology of Ti-W composite was observed and the local-restricted elemental composition was determined using scanning electron microscope and energy dispersive X-ray microanalysis (SEM-EDX, Hitachi S-5200). Absorption spectra of the photocatalysts were obtained with a diffuse reflectance UV-Vis spectrophotometer (JASCO V-600, Japan) equipped with an integrating sphere and were converted from reflection to absorbance by the Kubelka-Munk method. BET-specific surface area and the mean porous equivalent diameter were determined using a micrometrics automatic surface area analyzer and a porosimetry system (TriStar 3000, Shimadzu). A powder X-ray diffraction pattern (XRD) was obtained using an XRD diffractometer (Rigaku, Cu-Ka radiation) to examine the crystal structure of titania and tungsten trioxide.

2.3 Photocatalytic measurement

Photodegradation of MB is the most popular method for the evaluation of photocatalytic performance[21]. The photodegradation was conducted in a 100 mL quartz beaker with a suspension containing 50 mL of 25 $mmol{\cdot}m^{-3}$ MB aqueous solution and 20 mg photocatalyst. The initial pH value of the solution was fixed at 3. The suspension was agitated in darkness and then irradiated from underneath using a UV lamp (9.0 W, λmax = 365 nm) for UV irradiation and a lamp of projector (EPSON EB-1750, 230 W lamp, 2600 lm) for visible light irradiation. The distance between the light source and the beaker bottom was 10 mm. The concentration of MB was estimated by measuring the absorbance at 665 nm using a UV-Vis spectrophotometer. The adsorption amounts of MB on the photocatalysts were evaluated in darkness using the same experimental apparatus.

TiO_2 is well known adsorbent for the arsenic compounds. To evaluate the photo-reactivity of Ti-W photocatalyst, the photooxidation of As(III) was investigated with the same experimental procedures as described for the photodegradation of MB. The initial concentration of As(III) was fixed at 250 $mmol{\cdot}m^{-3}$. The concentrations of arsenic compounds were determined from the absorbance at 195 nm using HPLC equipped with a UV detector (TOSOH, 8020 series).

3. Results and discussion

3.1 Catalyst characterization

The absorption of visible light on Ti-W composites with the tungsten content of 30 wt% was found to be significantly strong compared to the composites with the tungsten content of 10 and 20 wt% Hereafter, the tungsten content in Ti-W composite was fixed at 30 wt%. Fig. 1 shows the powder XRD patterns of TiO_2 and Ti-W composites synthesized at the calcination temperature of 800°C. TiO_2 and Ti-W composites synthesized without IL ((a) and (b) in Fig. 1) exhibit both anatase and rutile peaks at 25.3° and 27.4°, respectively. This means the crystal phase transformation from anatase to rutile occurred at 800°C. Well defined three peaks around 24° corresponding to monoclinic WO_3 were clearly identified in any Ti-W compounds calcinated at 800°C. However no rutile peak was observed in Ti-W[PF_6] and Ti-W[BF_4] ((c) and (d) in Fig. 1). The TiO_2 inorganic network formed in sol-gel synthesis is not thermally stable enough to resist anatase-rutile crystal phase transformation during thermal treatment[23]. Owing to high thermal stability and high ion density of dispersed IL in TiO_2 sol-gel network, highly porous and thermally stable TiO_2 particles with anatase crystalline structure were formed at 800°C[20]. Although the WO_3 crystallization in Ti-W composites proceeded with increase in calcination temperature, the anatase-rutile phase transformation started above 800°C. Accordingly, the calcination temperature was fixed at 800°C.

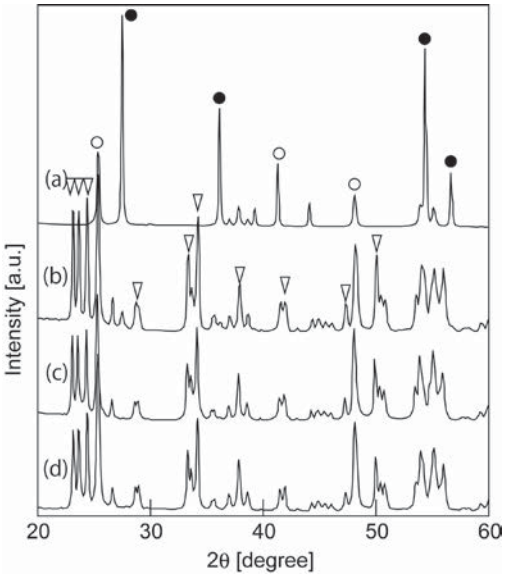

Fig. 1 XRD patterns of TiO_2 and Ti-W compounds, (a) TiO_2 synthesized without IL, (b) Ti-W compound synthesized without IL, (c) Ti-W[PF_6], (d) Ti-W[BF_4], ○; anatase TiO_2, ●; rutile TiO_2, ∀: tungsten trioxide, calcination temperature = 800 °C.

Table 1 Characterization of Ti-W composites (30 wt% WO_3-TiO_2).

Synthesis condition	Calcination temp. (°C)	Crystal phase TiO_2/WO_3	Pore volume ($cm^3 \cdot g^{-1}$)	BET surface area ($m^2 \cdot g^{-1}$)	D_{BJH} (nm)	CS_{XRD} (nm) TiO_2/WO_3	PS_{DLS} (nm)
Ti-W without IL	as-synthesized	Amor.*1/ Amor.	0.116	151	7.04	—	
	400	A.*2/Amor.	0.168	142	5.5	15.9/—	
	800	A. and R.*3/Mono.*4	0.057	17.1	26.1	32.0 / 46.5	389.5
Ti-W[PF_6]	as-synthesized	A./Amor.	0.15	24.65	—	4.62	
	400	A./Amor.	0.14	163	4.10	16.5	
	800	A./Mono.	0.08	16.6	26.6	31.4/45.5	274.0
Ti-W[BF_4]	as-synthesized	Amor./Amor.	—	0.09	—	—	
	400	A./Amor.	0.12	122	3.93	6.61	
	800	A./Mono.	0.04	10.53	42.66	41.8/57.6	173.5

*1, Amor.=amorphous, *2, A.=anatase, *3, R.=rutile, *4, Mon.=Monoclinic ; VD_{BJH}, BJH average pore diameter; CS_{XRD}, crystallite size measured from XRD; PS, particle size measured from DLS.

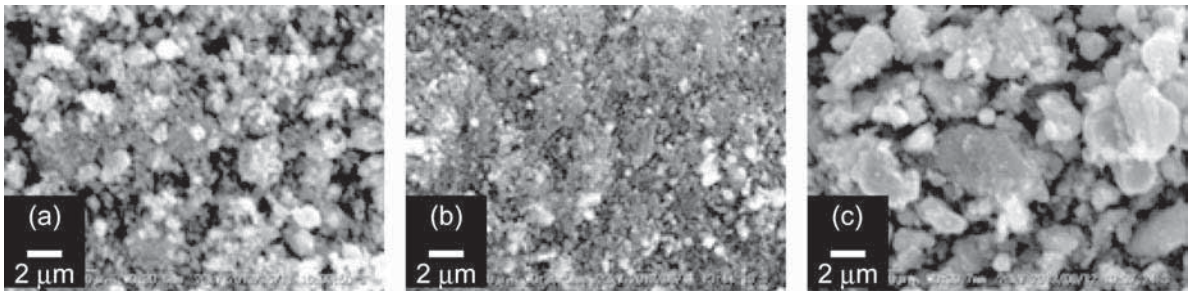

Fig. 2 SEM image of Ti-W compounds, (a): without IL, (b): Ti-W[PF_6], (c): Ti-W[BF_4].

Table 1 summarizes the pore volume, BET-specific surface area, average pore diameter and crystalline size of the synthesized Ti-W compounds. Ti-W[PF_6] indicated higher porosity and lower crystalline size than Ti-W[BF_4]. Water-miscible [Bmim][BF_4] might influenced the increase in mesopore size. However the agglomeration size determined with dynamic light scattering became small when [Bmim][BF_4] was used.

Fig. 2 shows surface morphology of Ti-W compounds. Fine powder was obtained for Ti-W[PF_6] compared to Ti-W compounds prepared without IL and Ti-W[BF_4] due to the formation of fine aqueous droplets in emulsion. From the SEM-EDX analysis, homogeneous distribution of WO_3 on Ti-W[PF_6] powder was confirmed.

Fig. 3 shows the diffuse reflectance spectrophotometry of Ti-W composites. For the comparison, the spectra of anatase TiO_2 and WO_3 powders were also indicated. Absorption in visible region is caused by the modification of TiO_2 with WO_3. However, low absorption of visible light was observed for Ti-W[PF_6] at the calcination temperature of 400°C ((a) in Fig. 3) due

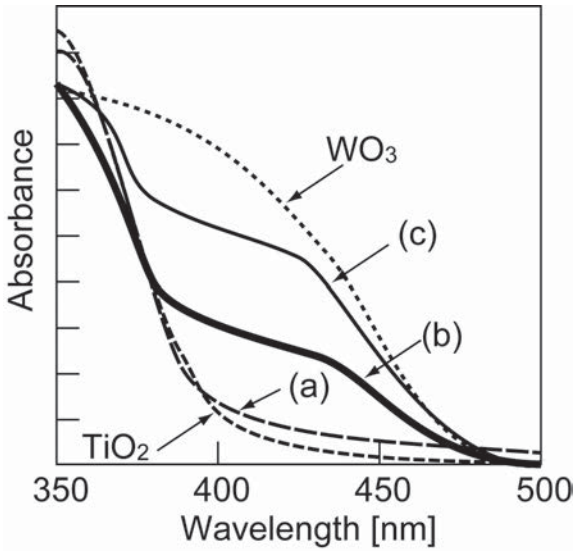

Fig. 3 Diffuse reflectance spectra of Ti-W compounds, (a) Ti-W[PF_6] at 400°C, (b) Ti-W[PF_6] at 800°C, (c) Ti-W[BF_4] at 800°C.

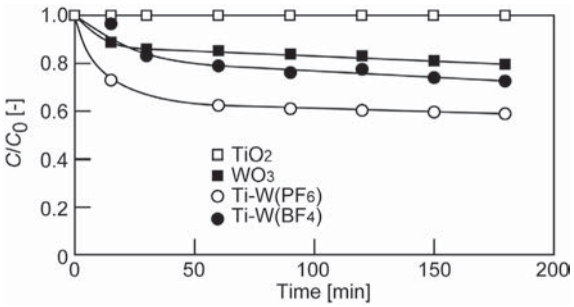

Fig.4 Adsorption of MB on TiO_2 (□), WO_3(■), Ti-W[PF_6] (○) and Ti-W[BF_4] (●).

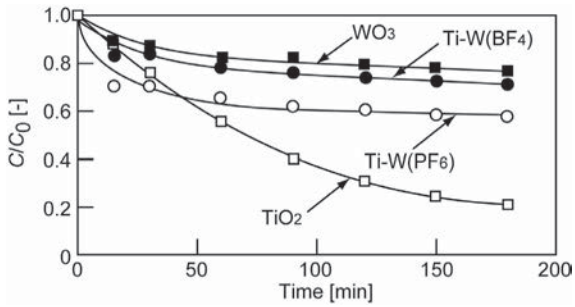

Fig.5 Photodegradation behavior of MB on Ti-W compounds under UV irradiation; TiO_2 (□), WO_3(■), Ti-W[PF_6] (○) and Ti-W[BF_4] (●).

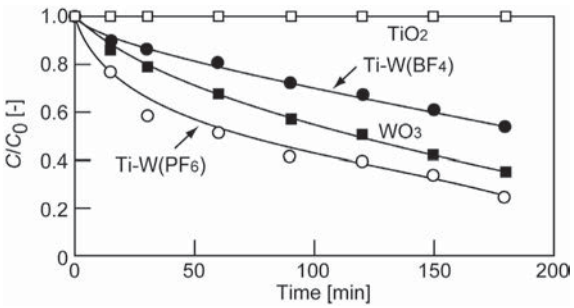

Fig. 6 Photodegradation behavior of MB on Ti-W compound under visible light irradiation; TiO_2 (□), WO_3(■), Ti-W[PF_6] (○) and Ti-W[BF_4] (●).

to the insufficient crystallinity of WO_3. Although there was little difference in crystallinity between Ti-W[BF_4] and Ti-W[PF_6] at the calcination temperature of 800°C as shown in Fig. 1, Ti-W[BF_4] with lower agglomeration size had better property than Ti-W[PF_6] as regarding the visible light absorption.

3.2 Photodegradation of methylene blue

Fig. 4 shows the adsorption behavior of MB on TiO_2, WO_3, Ti-W[PF_6] and Ti-W[BF_4]. There was no adsorption of MB on TiO_2 prepared by a sol-gel method [24]. The negative charged surface of WO_3 enhanced the adsorption of cationic MB. In addition, higher adsorption amount of MB was observed on Ti-W composites with high crystallinity compared to WO_3 powder calcinated at 800°C. Higher adsorption amount of MB was observed on Ti-W[PF_6] of the well dispersed WO_3 with BET surface area of 16.6 $m^2 \cdot g^{-1}$ compared to Ti-W[BF_4] powder with BET surface area of 10.5 $m^2 \cdot g^{-1}$. The adsorption amount of MB on Ti-W[PF_6] reached to 200 $mg \cdot g^{-1}$ under the condition of saturated adsorption.

Fig. 5 shows the photodegradation behavior of MB on TiO_2, WO_3, Ti-W[PF_6] and Ti-W[BF_4] under UV irradiation. The photodegradation behavior of MB on TiO_2 was clearly observed under UV irradiation. In this experiment, simultaneous adsorption and photodegradation of MB occurred on WO_3 nanoparticles. As might be expected, the WO_3 itself had no photocatalytic activity to MB degradation. The changes in MB concentration for Ti-W[PF_6] and Ti-W[BF_4] in Fig. 5 were almost same as those by adsorption of MB in Fig. 4. Thus the photodegradation rate of MB for Ti-W[PF_6] and Ti-W[BF_4] were found to be very low under UV irradiation, which might be caused by a mismatch between the site for the photocatalytic reaction on TiO_2 and that for the adsorption on WO_3.

Photodegradation behavior of MB under visible light irradiation was drastically changed compared with those under UV irradiation as shown in Fig. 6. The TiO_2 itself indicated no photodegradation of MB because of no absorption of visible light. Meanwhile photodegradation rate of MB on WO_3, Ti-W[PF_6] and Ti-W[BF_4] under visible light irradiation were much improved by combination effect of high adsorption of MB on the WO_3 surface and their ability to absorption of visible light. Although Ti-W[BF_4] had higher ability to absorb visible light than Ti-W[PF_6], Ti-W[PF_6] indicated higher photocatalytic activity for MB decomposition due to the high dispersive WO_3 nanoparticles.

3.3 Photooxidation of As(III)

Fig. 7 shows the adsorption behavior of As(III) and As(V) on the photocatalysts. WO_3 itself exhibited weakly adsorption of As(III) and no adsorption of As(V). As(V) adsorption on sol-gel synthesized TiO_2 was very much higher than As(III) adsorption at pH 3. Similar behaviors for adsorption of As(III) and As(V) on the TiO_2 prepared by hydrolysis of titanium sulfate and the commercial

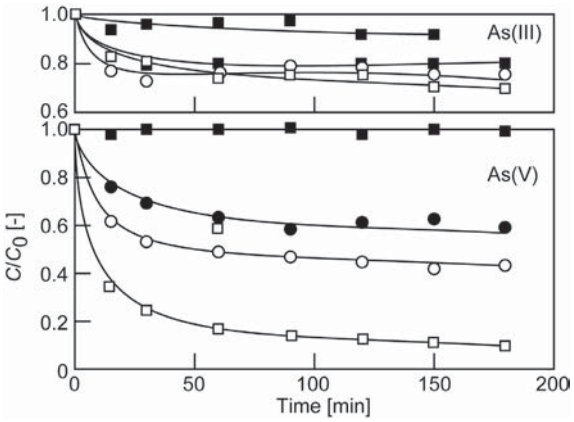

Fig. 7 Adsorption of As(III) and As(V); TiO_2 (□), WO_3(■), Ti-W[PF_6] (○) and Ti-W[BF_4] (●), concentration of As(III): 250 $mmol \cdot m^{-3}$, concentration of As (V): 250 $mmol \cdot m^{-3}$, pH 3.

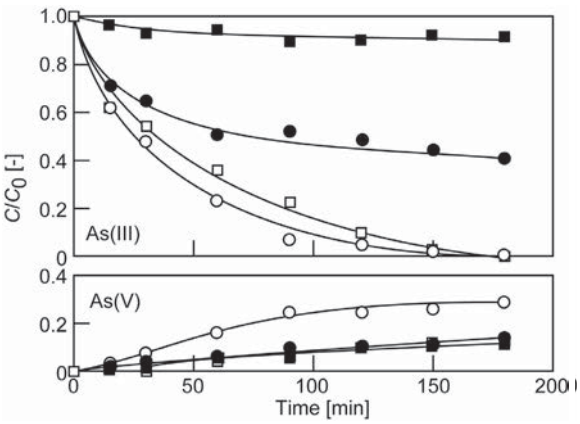

Fig. 8 Photooxidation of As(III) on Ti-W under UV irradiation; TiO_2 (□), WO_3(■), Ti-W[PF_6] (○) and Ti-W[BF_4] (●), concentration of As(III): 250 $mmol \cdot m^{-3}$, pH 3.

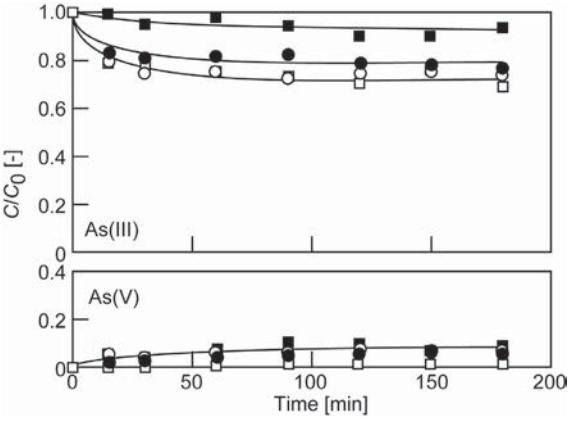

Fig. 9 Photodegradation of As(III) on Ti-W under visible light irradiation; TiO_2 (□), WO_3(■), Ti-W[PF_6] (○) and Ti-W[BF_4] (●), concentration of As(III): 250 $mmol \cdot m^{-3}$, pH 3.

TiO_2 have been reported[25, 26].

TiO_2 photocatalyst has been shown to effective in oxidizing As(III) to As(V)[27-30]. Photooxidation of As(III) on TiO_2 proceeds predominantly by reaction of As(III) with a superoxide radical or hydroxyl radical[27,28] (reactions 1 and 2). The resulting As(IV) is expected to be quickly oxidized to As(V) even by molecular oxygen (reaction 3).

$$As(III) + O_2^{\cdot -} + 2H+ \rightarrow As(IV) + HO_2^- \quad (1)$$
$$As(III) + OH^{\cdot} \rightarrow As(IV) + OH^- \quad (2)$$
$$As(IV) + O_2 \rightarrow As(V) + O_2^{\cdot -} \quad (3)$$

As shown in Fig. 8, As(III) concentration for Ti-W[PF_6] as well as TiO_2 was rapidly decreased to zero level after 3 hours under UV irradiation. Oxidized As(V) was successively adsorbed on the surface of TiO_2 and then the residual free As(V) in the solution was able to be detected. High photooxidation ability of As(III) on Ti-W[PF_6] would be caused by the effective charge separation and prevention of recombination of the electron-hole pair.

As shown in Fig. 9, Ti-W[PF_6] which was suitable as photocatalyst under UV irradiation exhibited a poor response to visible light for As(III) oxidation. There was no detection of As(V) in darkness during the adsorption test. However, a slight increase in As(V) concentration suggests the photooxidation of As(III) on Ti-W[PF_6] proceeds under visible light irradiation.

4. Conclusions

Highly dispersed Ti-W composite (Ti-W[PF_6]) was successfully prepared by a simple one-step sol-gel method with ionic liquid ([Bmim][PF_6]). The resulting Ti-W composites indicated high crystallinity of WO_3 and no crystalline transformation of TiO_2 from anatase to rutile with the assistance of IL. The combination of WO_3 and TiO_2 showed excellent properties to the visible light absorption. Photocatalytic activities of TiO_2, WO_3 and Ti-W photocatalysts were evaluated from photodegradation of methylene blue (MB) and photooxidation of As(III) both under UV and visible light irradiation. The Ti-W composites were ineffective for the degradation of MB under UV irradiation, which arose from a mismatch between the site for the photocatalytic reaction on TiO_2 and that for the adsorption on WO_3. Meanwhile, Ti-W[PF_6] indicated the highest photocatalytic activity in both the photodegradation of MB under visible light irradiation and the photooxidation of As(III) under UV irradiation.

Acknowledgement

This work was supported by a JSPS Grant-in-Aid for Challenging Exploratory Research (25630359), Japan.

References

1) R. Daghrir, P. Drogui and D. Robert, *Ind. Eng. Chem. Res.*, **52**, 3581 (2013).
2) M. Pelaez, N.T. Nolan, S.C. Pillai, M.K. Seery, P. Falaras, A.G. Kontos, P.S.M. Dunlop, J.W.J. Hamilton, J.A. Byrne and K. O'Shea, *Appl. Catal. B: Environ.*, **125**, 331 (2012).
3) H. Tong, S. Quyang, Y. Bi, N. Umezawa, M. Oshikiri and J. Ye, *Adv. Mater.*, **24**, 229 (2012).
4) H. Shen, L. Mi, P. Xu, W. Shen and P.-N. Wang, *Appl. Surf. Sci.*, **253**, 7024 (2007).
5) M. Shen, Z. Wu, H. Huang, Y. Du, Z. Zou, P. Yang, *Mater. Lett.*, **60**, 693-697 (2006).
6) D.Way, L. Xiao, Q. Luo, X. Li, J. An and Y. Duan, *J. Hazard. Mater*., **192**, 150 (2011).
7) M. Fujishima, Q. Jin, H. Yamamoto, H. Tada and M. Nolan, *Phys. Chem. Chem. Phys.*, **14**, 705 (2012).
8) T.-Y. Ma, Z.-Y. Yuan and J.-L. Cao, *Eur. J. Inorg. Chem.*, 716 (2010).
9) K. Maeda, M. Higashi, D. Liu, R. Abe and K. Domen, *JACS*, **132**, 5858 (2010).
10) Saepurahman, M.A. Abdullh and F.K. Chong, *J. Hazard. Mater.*, **176**, 451 (2010).
11) S.A.K. Leghari, S. Sajjad, F. Chen and J. Zhang, *Chem. Eng. J.*, **166**, 906 (2011).
12) S.A. Singh and G. Madras, *Sep. Purif. Technol.*, **105**, 79 (2013).
13) M. Ezaki, W. Michida, K. Kusakabe, *Adv. Mater. Res.*, in press, (2014).
14) P. Hapiot and C. Lagrost, *Chem. Rev.*, **108**, 2238 (2008).
15) D. Bradley, P. Dyson and T. Welton, *Chem. Rev.*, **9**, 18 (2000).
16) A. Vioux, L. Viau, S. Volland and J. Le Bideau, *C.R. Chimie*, **13**, 242 (2010).
17) L. Wang, S.-Z. Xu, H.-J. Li, L.-X. Chang, Zhi-Su, M.-H. Zeng, L.-N. Wang and Y.-N. Huang, *Journal of Solid State Chemistry* **184**, 720 (2011).
18) L. Wang, L. Chang, B. Zhao, Z. Yuan, G. Shao and W. Zheng, *Inorganic Chemistry*, **47**, 1443 (2008).
19) Li Wang, Li-Xian Chang, Lian-Qiang Wei, Shen-Zhi Xu, Ming-Hua Zeng and Shi-Lie Pan, *J. Mater. Chem.*, **21**, 15732 (2011).
20) H. Choi, Y.J. Kim, R.S. Varma and D.D. Dionysiou, *Chem. Mater.*, **18**, 5377 (2006).

21) R.J. Tayade, T.S. Natarajan and H.C. Bajaj, *Ind. Eng. Chem. Res.*, **48**, 10262 (2009).
22) M. Ferguson, M. Hoffmann and J. Hering, *Environ. Sci. Technol.*, **39**, 1880 (2005).
23) F. Bosc, A. Ayral, P.-A. Albouy, L. Datas and C. Guizard, *Chem Mater.*, **16**, 2208 (2004).
24) K. Kusakabe, M. Ezaki, A. Sakoguchi, K. Oda and N. Ikeda, *Chem. Eng. J.*, **180**, 245 (2012).
25) P.K. Dutta, A.K. Ray, V.K. Sharma and F.J. Millero, *J. Colloid Interf. Sci.*, **278**, 270 (2004).
26) M. Pena, X. Meng, G.P. Korfiatis and C. Jing, *Environ. Sci. Technol.*, **40**, 1257 (2006).
27) H. Yang, W.-Y. Lin and K. Rajeshwar, *J. Photoch. Photobio. A*, **123**, 69 (1999).
28) M.A. Ferguson, M.R. Hoffmann and J.G. Hering, *Environ. Sci. Technol.*, **39**, 1880 (2005).
29) P.K. Dutta, S.O. Pehkonen, V.K. Sharma and A.K. Ray, *Environ. Sci. Technol.*, **39**, 1827 (2005).
30) J. Ryu and W. Choi, *Environ. Sci. Technol.*, **40**, 7034 (2006).